Solid State Sciences 131 (2022) 106959

Contents lists available at ScienceDirect

Solid State Sciences

journal homepage: www.elsevier.com/locate/ssscie

Temperature-dependent dimerization of TCNQ anion-radical in $[Ni(bpy)_3]_2(TCNQ–TCNQ)(TCNQ)_2·6H_2O$: Single-crystal structure, magnetic and quantum chemical study

Slavomíra Šterbinská [a], Mariia Holub [b], Michal Hegedüs [a,1], Ján Titiš [c], Erik Čižmár [b], Larry R. Falvello [d], Juraj Černák [a,*]

[a] Department of Inorganic Chemistry, Institute of Chemistry, P. J. Šafárik University in Košice, Moyzesova 11, 041 54, Košice, Slovakia
[b] Institute of Physics, P. J. Šafárik University in Košice, Park Angelinum 9, 041 54, Košice, Slovakia
[c] Department of Chemistry, FPV, University of SS Cyril and Methodius, 917 01, Trnava, Slovakia
[d] Instituto de Nanociencia y Materiales de Aragón (INMA) and Departamento de Química Inorgánica, CSIC-Universidad de Zaragoza, Zaragoza, 50009, Spain

ARTICLE INFO

Keywords:
TCNQ
σ-Dimerization
Temperature-dependent crystal structure analysis
Nickel(II)
Magnetic properties
Quantum chemical calculations

ABSTRACT

The crystal structure of $[Ni(bpy)_3]_2(TCNQ–TCNQ)(TCNQ)_2·6H_2O$ (**1**) was studied by X-ray single-crystal structure analysis at 145 K and 100 K. The crystal structures of **1** at these two temperatures are essentially the same as the crystal structure studied previously at 200 K: the structure is built up of $[Ni(bpy)_3]^{2+}$ complex cations, two centrosymmetric crystallographically independent $TCNQ^-$ anion-radicals, disordered σ- and π-dimerized $(TCNQ)_2$ units, and water molecules of crystallization. Lowering the temperature from 200 K, via 145 K–100 K has shown that at lower temperatures the proportions of σ- and π-dimerization in the disordered $(TCNQ)_2$ unit are shifted in favor of σ-dimerization; moreover, variation of the weaker C–C σ-bond formed upon dimerization was observed. In addition, lowering the temperature led to a shortening of the distance between the two crystallographically independent anion-radicals which are stacked along the *b*-axis with overlapped exo groups. The σ- and π-dimerization in the disordered $(TCNQ)_2$ unit was studied by quantum chemical calculations which showed smallest energy difference for σ and π-dimer at 200 K with respect to 145 K and 100 K in line with a lowest proportion of the dimerization observed experimentally. Temperature-dependent (1.8–270 K) magnetic study of **1** has shown the contribution of Ni(II) ions ($S = 1$) and the contribution of four $S = 1/2$ species carried by TCNQ radicals at higher temperatures, strongly coupled by antiferromagnetic (AFM) exchange interaction at 270 K while at low temperature a negligible contribution of TNCQ radical spins was observed.

1. Introduction

TCNQ (7,7,8,8-tetracyanoquinodimethane) is a planar molecule (see Scheme 1) that can be easily reduced to form anion-radical $TCNQ^-·$ but for which its partial reduction is also possible; in this case usually an enhanced conductivity is observed [1–8]. $TCNQ^-·$ anion-radical (AR) in its reduced form has an unpaired electron and thus is magnetically active; this property is explored in the design of various magnetically active heterospin complexes mainly in combination with transition metals or lanthanides [4,9–16]. In these complexes the $TCNQ^-·$ AR, from a structural point of view, can play the role of a counter anion [11,17], or it can coordinate to central atom(s) in terminal or various bridging fashions [4,18,19]. Notable is the tendency of the $TCNQ^-·$ AR to dimerize or to form stacks interacting through π-electron clouds (π-dimerization) [20,21]. We note that such π-dimerization was observed also for other analogous species, like TCNE (TCNE = tetracyanoethylene) [22,23], or TCNB and TCNP (TCNB = 1,2,4,5-tetracyanobenzene, TCNP = 1,2,4,5-tetracyanopyrazine) [24]. More rarely, the proximity of two $TCNQ^-·$ ARs may lead to a σ-dimerization that manifests itself by forming a C–C σ-bond linking the two anions and resulting in a diamagnetic dianion $(TCNQ\text{-}TCNQ)^{2-}$ (Scheme 1, right).

A search in the CSD [25] has shown that there are 1199 hits for structures containing the TCNQ structural unit, 433 hits for compounds based on the combination of TCNQ with various transition metals or

* Corresponding author.
E-mail address: juraj.cernak@upjs.sk (J. Černák).
[1] Present address of M. Hegedüs: Synthon, s.r.o., Brněnská 32, 678 01 Blansko, Czech Republic.

https://doi.org/10.1016/j.solidstatesciences.2022.106959
Received 20 May 2022; Received in revised form 23 June 2022; Accepted 26 June 2022
Available online 4 July 2022

lanthanides; among these, in only 21 crystal structures a σ-dimerized dianion (TCNQ-TCNQ)$^{2-}$ was reported. As already noted above, the C–C σ-bond, linking the two TCNQ units is weaker than a normal C–C σ-bond and the observed bond distances range from 1.612 Å observed in *catena*-[Zn (TCNQ-TCNQ) (*bipy*)]·*p-xy* (*bipy* is 4,4′-bipyridine and *p-xy* is *p*-xylene; MUVHER) [26] to 1.673 Å found in [Pt (*bpy*)$_2$) (TCNQ-TCNQ)] (*bpy* = 2,2′-bipyridine, TCQDPT) [27].

Dimerization of radicals with the formation of a covalent C–C σ-bond is a well-known process studied within the field of dynamic covalent chemistry (DCC). Examples of dimerization of radicals include β-substituted (porphyrinyl)-dicyanomethyl radicals within the Ni(II) complex, which display reversible σ-dimerization in solution and were isolated as stable σ-dimers in the solid state with a C–C σ-bond of length 1.635 (1) Å [28], or the stable dimer based on *p*-dicyanomethyl--triphenylamine radical with a C–C σ-bond length of 1.616 Å [29]. Noteworthy is that Kobashi et al. [29] have suggested that a strong electron-donor group at the para-position weakens the bridging C–C bond in the dimeric form. An analogous dimerization process leading to C–C bond formation was reported for ionic fullerene compounds containing fullerene radical anions; these can form diamagnetic singly bonded dimers (C_{60}^{-})$_2$ and C ($_{70}^{-}$)$_2$ [30] which form fullerene salts with various *d*- and *f*-metals [31,32].

In our previous structural study of [Ni(*bpy*)$_3$]$_2$(TCNQ–TCNQ)(TCNQ)$_2$·6H$_2$O (**1**) [33] studied at 200 K, we have found that both π-dimerized ARs as well as σ-dimerized dianion (TCNQ-TCNQ)$^{2-}$ are present in this ionic complex. The experimental diffraction data were modelled assuming a simultaneous presence of the σ-dimerized dianion (TCNQ-TCNQ)$^{2-}$ (75.3 (9) %) and its π-dimerized form with two planar geometries of TCNQ units (24.7 (9) %). This model was adopted due to four arguments: (1) in the model assuming only a σ-dimerized dianion (TCNQ-TCNQ)$^{2-}$ (no disorder), the refined C–C distance was 1.878 (7) Å, which was outside the usual, above mentioned range; (2) the thermal ellipsoids of the pyramidalized carbon atoms were elongated along the C–C σ-bond; (3) near the pyramidalized carbon atom at a distance of 0.92 Å and positioned along the C–C bond a small local maximum of 0.58 *e*. Å^{-3} in the difference map was observed (the next highest maximum was 0.33 *e*. Å^{-3}), which might be interpreted as the position of the carbon atom of the π-dimerized form; and (4) in the disordered model (simultaneous presence of π- and σ-dimerized TCNQ's) the refined value 1.653 (11) Å of the C–C σ-bond fell within the established range. It should be noted that the program used for refinement did not suggest splitting of this pyramidalized C atom which forms a weaker σ-bond with its congener through the inversion center. The question remained open as to whether this disorder in the solid state exhibits a dynamic character (the rate of interconversion is more rapid than the data measurement time) or static (both geometries co-exist in different unit cells). In the case of the crystal structure of [Pt (*bpy*)$_2$] (TCNQ-TCNQ) (TCQDPT), in which the σ-dimerized dianion was reported for the first time, an enormous increase in paramagnetism at the transition temperature of 87 °C was observed [27]. Dong et al. [27], also considering the results of a previous magnetic study done by Endres et al. [34], have suggested that the C–C σ-bond breaks at this temperature, and the TCNQ radicals adopt their normal planar geometry.

In order to gain a better insight into the observed disorder between σ-dimerized and π-dimerized forms of the two TCNQ units we have undertaken a study of the crystal structure of [Ni(*bpy*)$_3$]$_2$(TCNQ–TCNQ)(TCNQ)$_2$·6H$_2$O at two different lower temperatures (145 K and 100 K). Additional theoretical calculations dealing with the bonding situation around the C–C σ-bond responsible for the dimerization were done, too, and the study was completed by variable temperature magnetic study of the title complex **1**. The obtained results are here reported here.

2. Experimental

2.1. Materials

Ni(NO$_3$)$_2$·6H$_2$O, LiI, TCNQ, 2,2′-bipyridine and methanol were purchased from commercial sources and used as received.

2.2. Synthesis

Complex **1** was synthetized according to the procedure described in the literature [33].

2.3. Single-crystal X-ray diffraction

X-ray experiments were carried out on a four-circle κ-axis Xcalibur 2 diffractometer equipped with a Sapphire 3 CCD detector (Oxford Diffraction). The CrysAlis software package [35] was used for data collection and reduction. The data for **1** were collected at two temperatures, 100 K and 145 K. As a starting model, the coordinates of the respective atoms from the refinement of data measured at 200 K were used [33]. Refinement based on intensities was performed using *SHELXL-2018/3* [36]. All non–hydrogen atoms were refined anisotropically using the same approach as in the published paper with the differences being that the thermal parameters for positions O3A and O3B were taken as common and their s.o.f.s were refined. As the data for **1** gathered at 100 and 145 K (**1–100** and **1–145**, resp.) were taken from a twinned crystal, the final refinement was conducted using data from both domains (hklf 5). The refinements for data at 100 K and 145 K were done in a like manner as for the structure determination for data measured at 200 K [33], i.e., assuming positional disorder of some atoms in the (TCNQ)$_2^{2-}$ dianion leading to the simultaneous presence of both σ- and π−dimerized {TCNQ}$_2$ units. Crystal data and final parameters for the structure refinements are summarized in Table 1. The structural figures (Figs. 1–4 and Figs. S1-S7) were drawn using Diamond [37].

In addition, we performed refinement calculations using a non-disordered approach in the case of the (TCNQ)$_2$ unit. The final refinement data are gathered in Table S1 in the Supplementary material, and the figures displaying the thermal ellipsoid plot of the dianions are shown in Figs. S5-S7.

2.4. Quantum-chemical calculations

Quantum-chemical calculations were performed with ORCA 4.1.2 computational package at the experimental geometries of the dimerized units, as well as optimized structures [38]. The relativistic effects were included in the calculations with zero order regular approximation (ZORA) together with the scalar relativistic contracted version of def2-TZVP basis functions for all elements. In DFT calculations

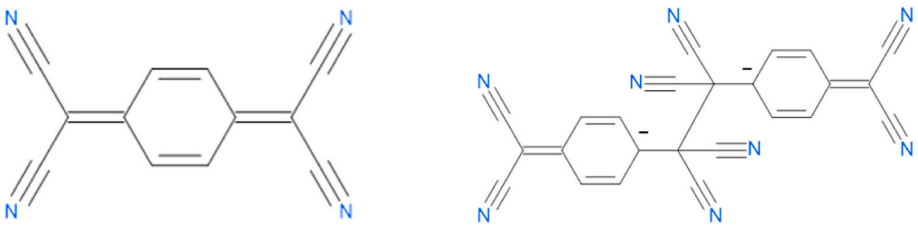

Scheme 1. Molecule of TCNQ (left) and σ-dimerized (TCNQ-TCNQ)$^{2-}$ dianion (right).

Table 1
Crystal data of $[Ni(bpy)_3]_2(TCNQ–TCNQ)(TCNQ)_2{\cdot}6H_2O$ (**1**) for structures at different temperatures, **1–200**, **1–145**, and **1–100**, resp. The data for **1–200** were taken from publications [33].

	1–100	1–145	1–200
Empirical formula	C108 H76 N28 Ni2 O6	C108 H76 N28 Ni2 O6	C108 H76 N28 Ni2 O6
Molecular weight	1979.35	1979.35	1979.35
Crystal system	Triclinic	Triclinic	Triclinic
Space group	*P*-1	*P*-1	*P*-1
Unit cell dimensions			
a (Å)	12.3479 (12)	12.3712 (10)	12.4034 (4)
b (Å)	13.1652 (13)	13.2198 (11)	13.2921 (4)
c (Å)	15.2606 (13)	15.3526 (11)	15.4869 (4)
α (°)	88.969 (8)	88.915 (6)	88.828 (3)
β (°)	85.734 (8)	86.021 (6)	86.336 (3)
γ (°)	73.611 (8)	73.426 (7)	73.586 (3)
V (Å^3)	2373.4 (4)	2400.7 (3)	2444.21 (13)
Z	1	1	1
D_{calc} (Mg.m^{-3})	1.385	1.369	1.345
Temperature (K)	100 (2)	145 (2)	200 (2)
μ (mm^{-1})	0.471	0.465	0.457
Crystal dimensions (mm)	0.586 × 0.342 × 0.283	0.586 × 0.342 × 0.283	0.520 × 0.391 × 0.277
F (000)	1024	1024	1024
Index ranges	$-14\leq h\leq 14$ $-15\leq k\leq 15$ $-18\leq l\leq 18$	$-15\leq h\leq 14$ $-16\leq k\leq 16$ $-18\leq l\leq 18$	$-16\leq h\leq 16$ $-18\leq k\leq 17$ $-20\leq l\leq 19$
θ range (°)	4.45–25.02	4.56–25.68	2.91–28.97°
Reflections collected	10211	14151	31246
Independent reflections	10211	14151	11255
Independent reflections	($I > 2\sigma_I$) 6354	7477	7475
Goodness-of-fit on F^2	1.062	1.000	1.047
R indices ($I > 2\sigma_I$)	$R_1 = 0.0742$ $wR_2 = 0.2054$	$R_1 = 0.0744$ $wR_2 = 0.2079$	$R_1 = 0.0492$ $wR_2 = 0.1260$
R indices (all data)	$R_1 = 0.1170$ $wR_2 = 0.2247$	$R_1 = 0.1317$ $wR_2 = 0.2295$	$R_1 = 0.0910$ $wR_2 = 0.1071$
Diff. Peak and hole (e.Å^{-3})	0.838; −0.883	0.656; −0.970	0.336; −0.244

(single-point and geometric optimization) the hybrid B3LYP/D3 exchange-correlation functional (with dispersion correction using Becke-Johnson damping) was used. The calculations utilized the RI approximation with appropriate decontracted auxiliary basis set and the chain-of-spheres (RIJCOSX) approximation to exact exchange. Increased integration grids (Grid 4 and GridX5) and tight SCF convergence criteria were used. DLPNO-CCSD calculations were used for local energy decomposition (LED) of interaction energy between the two crystallographically independent anion-radicals in π-dimers as implemented in ORCA package [39]. TightPNO settings were used.

2.5. Magnetic measurements

Susceptibility (estimated as the ratio of measured magnetic moment and applied magnetic field) and magnetization were measured on a commercial Quantum Design MPMS3 magnetometer in the temperature range from 1.8 to 270 K in magnetic fields up to 7 kOe. Due to a possible release of crystalline water, a nascent polycrystalline specimen stored initially in a freezer was installed in a polypropylene VSM capsule and quickly cooled in the sample chamber of the magnetometer at the rate of 25 deg/min. During the measurement, the sample temperature was kept below 270 K. The diamagnetic contribution of the sample holder and sample itself (estimated using Pascal's constants) was subtracted. A typical value of the temperature-independent paramagnetism (TIP) of Ni (II) ion of $\chi_{TIP} = 100 \times 10^{-6}$ emu/mol was also subtracted.

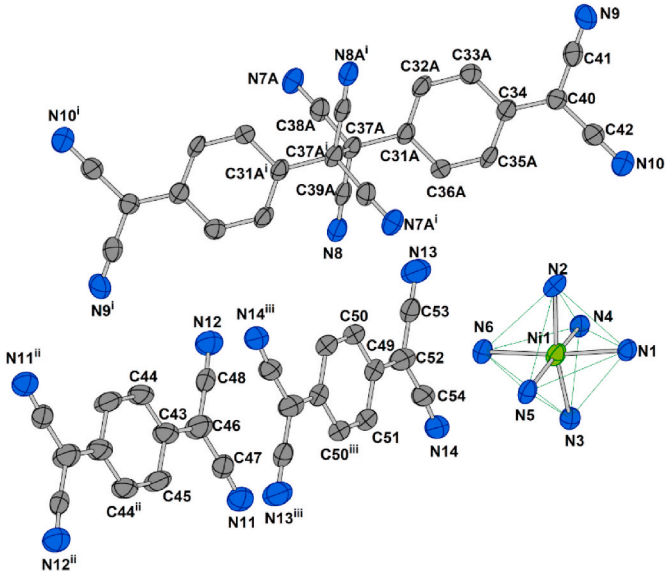

Fig. 1. View of the crystal structure of **1** at 100 K showing the main building units along with the atom numbering scheme. Among the σ- and π-dimerized $(TCNQ)_2$ units only the σ-dimerized one is shown for clarity. The complex cation is shown as a polyhedron for the sake of clarity; for the same reason the solvate molecules of water are omitted. The thermal ellipsoids are drawn at the 50% probability level. Symmetry codes: (i) 1 - x, 1 - y, 2 - z; (ii) 1 - x, 2 - y, 1 - z; (iii) 1 - x, 1 - y, 1 - z.

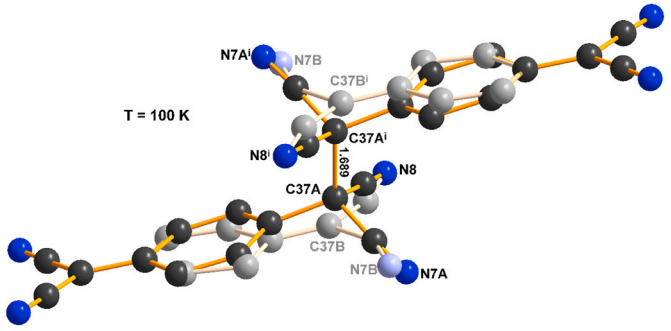

Fig. 2. Disordered dimerized $(TCNQ)_2$ units formed by σ-dimerized $(TCNQ–TCNQ)^{2-}$ dianions and by a pair of $TCNQ^{\cdot-}$ anion-radicals, π-dimerized through their exocyclic groups, at a temperature of 100 K. Hydrogen atoms are omitted for clarity. The less populated positions are shown with weaker coloration. Symmetry code: (i) 1 - x, 1 - y, 2 - z.

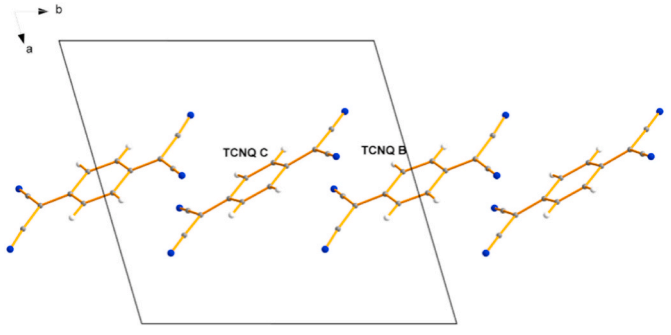

Fig. 3. View of the stacking of ARs denoted TCNQB and TCNQC in **1** at 100 K.

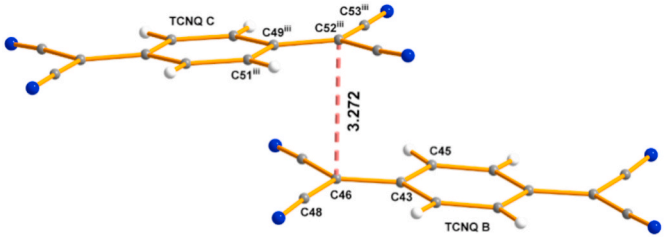

Fig. 4. Detailed view of the overlap of two ARs TCNQB and TCNQC in **1** at 100 K. Symmetry code: iii: 1-x, 1-y, 1-z.

3. Results and discussion

3.1. Crystal structure of *1*

The crystal structure of **1** studied at 200 K was already reported in our previous study [33]. The main features of the crystal structure of **1** at all three studied temperatures (200, 145, and 100 K) are the same as those reported for the structural study at 200 K [33], so here we report only the main features of the structure and emphasis will be placed on the temperature-dependent features. The crystal structure of **1** is built up of $[Ni(bpy)_3]^{2+}$ complex cations, centrosymmetric $(TCNQ)_2$ σ- and/or π-dimerized units, additional crystallographically independent $TCNQ^{\cdot-}$ ARs, and water molecules of crystallization (Fig. 1, Figure S1).

The remarkable feature of the crystal structure of **1** is the presence of a $(TCNQ)_2$ dimeric unit (TCNQA). The results of structural refinements suggest that this dimeric unit is disordered. The observed disorder was modelled assuming the presence of both the $(TCNQ)_2^{2-}$ dianion, in which the two parts are linked by a C–C σ-bond, and a π-dimerized pair of $TCNQ^{\cdot-}$ ARs. Although this disorder was observed at all three studied temperatures (Fig. 2, Figure S2), the refinements using this model led to somewhat different proportions of the two forms of the $(TCNQ)_2$ dimeric unit at the different temperatures. The values of the calculated site occupation factors, along with the values of the C–C σ-bond distances, are gathered in Table 2. We note that an increase was observed in the distance C37A···C37A^{i}, from 1.689 (10) Å at T = 100 K to 1.746 (10) Å at T = 145 K. This appears to be part of a more extended expansion in that direction; we note that the distance C37B···C37B' increases from 3.12 (6) Å at T = 100 K to 3.34 Å at T = 145 K. Our conjecture is that there may be a minor thermal transition that gives this expansion in that direction. Interpretation of this observation should take into account the presence of extended disorder in the crystal structure accompanied by twinning of the crystal. We further note that the X-ray data at T = 100 K and T = 145 K were taken from the same crystal (100 K first), while the data at T = 200 K were from a different crystal. Because of the twinning and disorder in the crystal measured at two temperatures, with possibly mobile domain boundaries, it could be that different samples respond differently to changes in temperature.

As can be seen from Table 2, at both lower temperatures, 145 K and 100 K, the single-crystal X-ray experiments yielded a significantly higher proportion of the $(TCNQ)_2^{2-}$ dianion (about 89%) with respect to the π-dimerized form of two $TCNQ^{\cdot-}$ ARs, than was reported for the temperature of 200 K (75%). As to the C–C bond of the σ-dimerization (C37A-C37A^{i}; i: 1-x, 1-y, 2-z) this was found to be within the range 1.653 (11)-1.746(10) Å; all observed values are longer than the normal single bond. The values at 100 K and 200 K correspond well to values observed in analogous complexes, e.g. a value of 1.645 (7) Å was reported for [Fe(*phen*)$_3$](TCNQ)$_2$ [11]. On the other hand, this bond is significantly longer at 145 K, with a value of 1.746 (10) Å. We have no ready explanation at present for this observation. It may result from a rearrangement within the structure at temperatures close to this one.

We note that we have also examined the possibility that the dimerized $(TCNQ)_2^{2-}$ dianion is not disordered. The refinement results and the thermal ellipsoid plot are given in the Supplementary material (Table S1, Figs. S5-S7). As can be seen from these figures, the thermal ellipsoid of the carbon atoms of the σ-dimerization are strongly elongated along the bonds, and additional peaks were localized in the difference map on the assumed sites for these carbon atoms in the case of π-dimerization. In addition, the theoretical calculations favored the disordered model (see part 3.2).

Selected geometric parameters are gathered in Table 3 and Table S2. The ranges for Ni–N bond distances are 2.078 (2) - 2.1093 (19) Å (200 K), 2.063 (3) - 2.109 (3) Å (145 K) and 2.064 (4) - 2.107 (3) Å (100 K) and these indicate only minor shortening of the Ni–N bond distances due to lowering the temperature as expected due to the rigidity of the Ni(II) coordination sphere. We note that at all three temperatures, the shortest Ni–N bond is that of Ni–N6 while the longest one is, in all cases, the Ni–N2 bond. Similar ranges for Ni–N bonds were found in analogous Ni(II) complex cations with dimethylderivates of the *bpy* ligand [17].

The C–C bonds in the respective TCNQ units exhibit different characters, and some of them display a tendency to aromatization. We note

Table 2
Site occupation factors for the two forms of dimerized $(TCNQ)_2$ units and the C–C distances [Å] in σ-dimerized $(TCNQ)_2^{2-}$ dianon.

Temperature [K]	sof [%]		σ-dimerized	References
	σ-dimerized	π-dimerized	C–C bond [Å]	
100	88.4 (4)	11.6 (4)	1.689 (10)	this work
145	89.8 (4)	10.2 (4)	1.746 (10)	this work
200	75.3 (9)	24.7 (9)	1.653 (11)	Černák, 2017

Table 3
Selected geometric parameters [Å, °] for **1** at three temperatures. In this table are included only values related to the more populated atoms in the case of disorder.

Bond [Å]/angles [°]	200 K	145 K	100 K
Complex cation			
Ni1–N1	2.0897 (19)	2.094 (3)	2.086 (3)
Ni1–N2	2.1093 (19)	2.109 (3)	2.107 (3)
Ni1–N3	2.0945 (19)	2.089 (3)	2.087 (3)
Ni1–N4	2.103 (2)	2.101 (3)	2.093 (3)
Ni1–N5	2.084 (2)	2.093 (3)	2.077 (3)
Ni1–N6	2.078 (2)	2.063 (3)	2.064 (4)
N1–Ni1–N2	78.61 (7)	78.73 (13)	78.81 (14)
N3–Ni1–N4	78.47 (7)	78.87 (13)	79.02 (13)
N5–Ni1–N6	78.69 (8)	79.33 (12)	79.15 (13)
TCNQA			
C31A–C32A	1.422 (8)	1.387 (7)	1.387 (8)
C32A–C33A	1.390 (2)	1.386 (6)	1.384 (6)
C33A–C34	1.412 (6)	1.418 (6)	1.411 (6)
C34–C35A	1.410 (6)	1.396 (6)	1.412 (6)
C35A–C36A	1.375 (6)	1.382 (6)	1.364 (6)
C31A–C36A	1.405 (9)	1.408 (7)	1.391 (7)
C31A–C37A	1.527 (7)	1.533 (7)	1.538 (7)
C37A–C38A	1.485 (4)	1.475 (6)	1.472 (6)
C37A–C39A	1.477 (6)	1.461 (7)	1.455 (7)
C37A–C37A^{i}	1.653 (11)	1.746 (10)	1.690 (10)
C34–C40	1.440 (3)	1.445 (6)	1.421 (6)
C40–C41	1.398 (3)	1.395 (6)	1.401 (6)
C40–C42	1.411 (3)	1.419 (6)	1.421 (6)
TCNQB			
C43–C44	1.416 (3)	1.400 (6)	1.391 (7)
C43–C45	1.421 (3)	1.423 (5)	1.425 (6)
C44^{ii}–C45	1.352 (4)	1.361 (6)	1.366 (7)
C43–C46	1.418 (4)	1.417 (6)	1.422 (7)
C46–C47	1.412 (4)	1.404 (7)	1.392 (7)
C46–C48	1.424 (4)	1.424 (6)	1.426 (6)
TCNQC			
C49–C50	1.417 (4)	1.416 (7)	1.386 (7)
C49–C51	1.421 (3)	1.425 (6)	1.427 (6)
C50^{iii}–C51	1.359 (4)	1.369 (7)	1.375 (7)
C49–C52	1.415 (4)	1.413 (7)	1.445 (8)
C52–C53	1.412 (4)	1.424 (6)	1.411 (7)
C52–C54	1.422 (4)	1.419 (7)	1.376 (8)

Symmetry codes: i: 1 - x, 1 - y, 2- z, ii: 1 -x, 2 - y, 1 - z, iii: 1 - x, 1 - y, 1 - z.

that the highest differences in bond distances due to different temperatures were found for C31–C32 and C52–C54 bonds with values of 0.035 and 0.046 Å, respectively (Table 3, Fig. 1); the differences in C–C bond distances for other bonds are usually much smaller.

As to the supramolecular structure of **1**, its detailed description was provided in our previous paper [33]. Here we will pay attention to the stacking mode of the centrosymmetric TCNQB (contains atom C43) and TCNQC (contains atom C49) ARs (Fig. 3, Figure S3, Fig. 4, and Figure S4) as these are important for the interpretation of the observed magnetic properties (see below). From Fig. 3 (Figure S3), it follows that the ARs TCNQB and TCNQC are stacked along the *b* axis by an "external bond over external bond" fashion; for nomenclature, see Ref. [4], i.e., these two TCNQ ARs exhibit an overlap by their exo groups (Fig. 4 and Figure S4). The shortest distance between these two ARs at 100 K is represented by a contact of 3.272 (9) Å between the C46 (TCNQB) and C52^{iii} (TCNQC; iii: 1-x, 1-y, 1-z) atoms, and this distance becomes longer with elevated temperature up to 3.397 (4) Å at 200 K (Fig. 4, Table 4). We note that in the $(TCNQA)_2$ unit, the π-interacting TCNQ's exhibit analogous overlap, and the corresponding C37B···C37B^{i} (i: 1-x, 1-y, 2-z) interatomic distances are 3.119 (5) and 3.335 (6) Å for T = 100 and T = 145 K, respectively. It is worth noting that the exo groups in the respective ARs TCNQB and TCNQC are not exactly coplanar with the quinoide rings, and similarly, the respective quinoide rings are not coplanar as well (Table 4). The highest deviation exists at 200 K, and it can be seen that the neighboring ARs are more closely placed with lowering the temperature. Consequently, this may reinforce exchange coupling between the two ARs manifesting itself in lowering the magnetic response at lower temperatures.

3.2. Quantum chemical calculations

In order to obtain a better insight into the crystal structure of **1**, we have performed quantum-chemical calculations for TCNQ dimers in crystal structures experimentally obtained at three different temperatures. First of all, at the level of B3LYP-D3/ZORA-def2-TZVP theory, we have visualized molecular orbitals that mediate the interactions of individual TCNQ monomers in given dimeric structures in the form of intrinsic bond orbitals (IBOs) [40]. The results are shown in Fig. 5. In dimer $(TCNQ–TCNQ)^{2-}$, the C–C bond between the monomers is formed by a σ bonding molecular orbital with electron population 1.896. The bond order is 0.81. In the case of dimer $(TCNQ^{\cdot-})_2$, the interaction is mediated by a weak overlap of the π molecular orbitals located on the exo groups of the individual TCNQ ARs.

In the next part of our analysis, we relied on calculations at the level of DLPNO-CCSD theory, which provided reliable energies of the solved systems. These were subsequently used in LED (localized energy decomposition) analysis, the purpose of which was to determine the interaction energy of TCNQ monomers in the dimers in question. The results are summarized in Table 5. The total electronic energies of σ-dimeric structures at temperatures of 100, 145 and 200 K are: E_{tot}/a.u. −1352.119, −1352.113 and −1352.127, respectively. In the case of π-dimeric structures, the energies are, as expected, higher: E_{tot}/a.u. −1352.086, −1352.089 and −1352.108. The energy difference between σ and π-dimers is smallest at 200 K, compared to lower temperatures, which corresponds to a decrease in the proportion of the dimerization observed experimentally.

The LED analysis of the interaction energy between the two crystallographically independent ARs in π-dimers revealed the temperature dependence of ΔE_{int}, which is obviously related to the observed shortening of the distance between the C atoms of exo groups in terms of lowering the temperature. The largest interaction energy was calculated for the structure at $T = 100$ K, with the most significant contributions to this value being electrostatic interaction and electronic preparation energy. These conclusions are fully consistent with the calculations of Miller et al. [24,41]. Based on the results of DFT and *ab initio* multireference methods, the repulsive interaction for TCNQ·– TCNQ·- system was confirmed (large positive $E_{el\text{-}stat}$ values in our calculations). In addition, the stability of the π-dimer in solid state was attributed to the interaction with the appropriate cation.

3.3. Magnetic properties

The magnetic properties of **1** were studied in the temperature range 1.8–270 K. The value of the effective magnetic moment of **1** at 270 K, $\mu_{eff} = 4.828\ \mu_B$ (μ_B is Bohr magneton), corresponds to $\chi T = 2.915$ emuK/mol as shown in Fig. 6, reflects the contribution of two Ni(II) ions ($3d^8$, spin $S = 1$) present in the molecular unit in the paramagnetic limit including the contribution of four $S = 1/2$ species carried by TNCQ radicals at higher temperature range, strongly coupled by antiferromagnetic (AFM) exchange interaction. At low temperatures, a drop of μ_{eff}/μ_B was observed that could be caused by an axial single-ion anisotropy (eventually some a weak AFM exchange interaction). No difference between zero-field cooled and field cooled magnetic response of **1** was observed to indicate possible long-range magnetic order down to 1.8 K. The low-temperature magnetization is fully compatible with the presence of two isolated Ni(II) ions in $[Ni(bpy)_3]^{2+}$ cation and negligible contribution of TNCQ radical spins. The magnetization value of 4.424 $N_A\mu_B$ at 1.8 K and 7 kOe is close to the saturation value of magnetization of two Ni(II) ions with a typical *g*-factor of 2.22. The difference between the magnetization measured at the lowest temperatures shown in Fig. 7 in reduced coordinates suggests the presence of a small single-ion anisotropy defined in the effective spin Hamiltonian using parameters *D* and *E* and a Zeeman term in the form

$$\widehat{\mathscr{H}}_{ZFS} = D\left[\widehat{S}_z^2 - S(S+1)/3\right] + E\left[\widehat{S}_x^2 - \widehat{S}_y^2\right] + \mu_B \widehat{S}\overline{\overline{g}}\widehat{H}. \quad \text{(Eq. 1)}$$

Since the correct determination of the sign of a small single-ion anisotropy from the analysis of the magnetic response of polycrystalline sample may be ambiguous, simple *ab initio* calculations were performed in ORCA on the isolated $[Ni(bpy)_3]^{2+}$ cation using atomic coordinates determined by an X-ray study. The SA-CASSCF/NEVPT2 calculations in the case of CAS (8,5) active space yield a negative value of the axial $D/k_B = -3.73$ K and rhombic $E/D = 0.076$ parameter of the single-ion anisotropy. The obtained value of *D* was set as a starting value in the following analysis of the experimental data, and a small *E* was omitted to avoid over-parameterization. First, the field dependence of magnetization at 1.8 K was fit to a simple model according to Eq. (1) with $E = 0$. The calculation of magnetization was performed using the EasySpin [42] toolbox in the MATLAB environment. The average magnetic response was calculated from the distribution of the magnetic-field vector over the orientational grid to account for the polycrystalline characteristics of the sample. The fit shown in Fig. 7 by a solid line yielded $D/k_B = -3.71$ K and an average *g*-factor $g_{Ni} = 2.25$, close to the predicted values from SA-CASSCF/NEVPT2 calculations.

To analyze the temperature dependence of χT, the contribution of TCNQ radicals at higher temperatures needs to be taken into account. From the crystal structure, two different contributions of TCNQ ARs can be expected: from dominant σ-dimerized dianions $(TCNQ)_2^{2-}$ (TCNQA

Table 4
Geometric parameters associated with stacking of ARs TCNQB and TCNQC at different temperatures. Values for T = 200 K taken from Ref. [33]. Symmetry code, iii: 1 -x, 1 - y, 1 – z.

Temperature/K	τ1/°	τ2/°	τ3/°	d/Å
200	175.9 (2)	−179.9 (2)	9.42 (8)	3.397 (4)
145	177.7 (5)	−179.7 (5)	10.41 (4)	3.332 (7)
100	176.9 (5)	180.0 (5)	9.56 (4)	3.272 (9)

τ1: torsion angle C45–C43–C46–C48.
τ2: torsion angle C51–C49–C52–C53.
τ3: angle between the quinoide rings of TCNQB and TCNQC.
d: distance between atoms C46 and C52^{iii}.

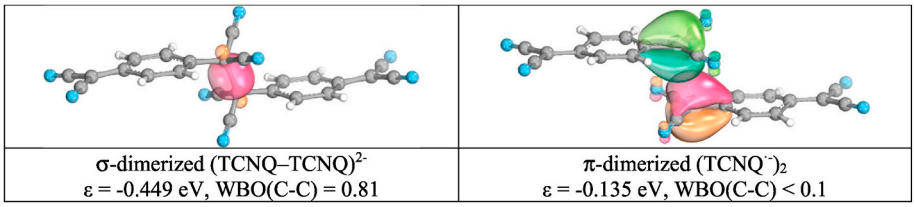

Fig. 5. Calculated intrinsic bond orbitals (B3LYP-D3/def2-TZVP) in dimers (T = 200 K) responsible for σ-bond and π–π interaction between TCNQ ARs (ε – orbital energy, WBO – Wiberg bond order).

Table 5
Localized energy decomposition for π-dimer $(TCNQ^{\cdot-})_2$.

Temperature/K	ΔE_{int}	$\Delta E_{g\text{-}p}$	$\Delta E_{el\text{-}p}$	$E_{el\text{-}stat}$	E_{ex}	ΔE_{ndisp}	E_{disp}
100	−9.35	2.54	−12.76	10.11	−10.42	9.47	−8.29
145	−2.58	2.01	−10.44	14.33	−8.87	7.96	−7.57
200	−1.14	2.11	−11.73	15.98	−7.53	8.97	−8.94

ΔE_{int} – interaction energy, $\Delta E_{g\text{-}p}$ – geometry preparation energy (energy penalty for the monomers to distort into the geometry of the dimer), $\Delta E_{el\text{-}p}$ – electronic preparation energy, $E_{el\text{-}stat}$ – electrostatic contribution, E_{ex} – exchange contribution, ΔE_{ndisp} – non-dispersive correlation contribution, E_{disp} – dispersive contribution. Energies in kcal mol^{-1}.

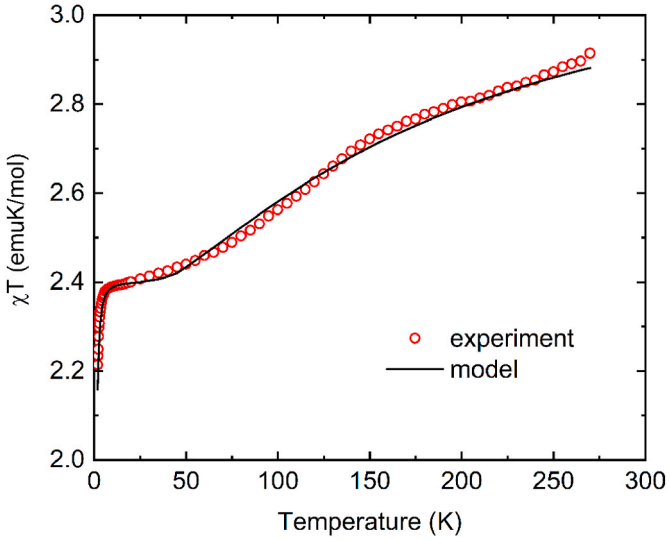

Fig. 6. The temperature dependence of χT of **1** (open symbols) measured in the applied field of 1 kOe, including the model proposed in the text.

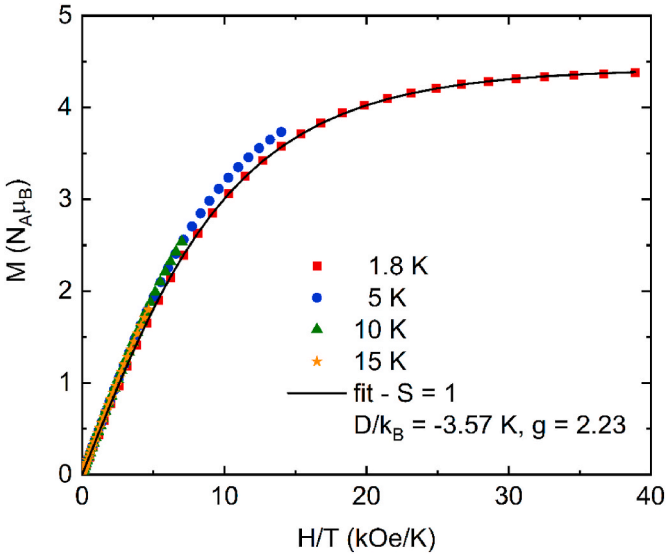

Fig. 7. The field dependence of the magnetization of **1** at 1.8 K, 5 K, 10 K, and 15 K (full symbols), including the fit of the spin Hamiltonian model at 1.8 K (solid line) in reduced coordinates.

type) and from stacks of crystallographically independent $TCNQ^{\cdot-}$ ARs (TCNQB and TCNQC type). The contribution of σ-dimerized dianions $(TCNQ)_2^{2-}$ in our experimental temperature range might be negligible, as suggested by the value of the activation energy of 0.25 eV (≈2900 K) to excite singlet ground state to the excited triplet state of AFM spin dimer in TCQDPT [27]. TCNQB and TCNQC ARs in the stacks along the crystallographic *b*-axis reside on inversion centers suggesting a uniform spin chain model for the analysis of magnetic properties. The proposed model to describe the susceptibility of a molecular unit of **1** in the temperature range 1.8–270 K is written in the form

$$\chi = 2\chi_{ZFS} + 2\chi_{chain} + \chi_0 \quad \text{(Eq. 2)}$$

and consists of χ_{ZFS} resulting from Eq. (1) for the contribution of two Ni (II) ions, χ_{chain} for the contribution of two TCNQ spins in stacks, and χ_0 for a possible correction to the estimated temperature-independent corrections (TIP, diamagnetic susceptibility, and a possible Pauli paramagnetic susceptibility at higher temperatures due to usual semiconducting character of AR salts). The high-temperature series expansion (HTSE) formula for dimerized (bond-alternating) AFM spin chain with parameter J for exchange coupling and α for the dimerization [43,44] was chosen to represent χ_{chain}; it transforms into a uniform spin chain model for $\alpha = 1$ [45–46]. Although HTSE formulas used for the analysis are valid with good accuracy for $k_BT > 0.25J$, the contribution of the dimerized or uniform spin chains to the χT for large values of J is expected to be negligible in comparison with the contribution of Ni(II) ions below $k_BT = 0.25J$. The contribution of χ_{ZFS} was again calculated using the EasySpin toolbox and combined with the HTSE formula for the dimerized spin chain. Although there is no significant structural dimerization of $TCNQ^{\cdot-}$ ARs in stacks, the simple uniform spin chain model failed to describe the high-temperature increase of χT, and the dimerization α was allowed to vary in further analysis. In general, a fair agreement of the experimental data with Eq. (2) was obtained for $D/k_B = -3$ K, $g_{Ni} = 2.19$ for $S = 1$ subsystem of Ni(II) ions and $J/k_B = 260$ K, and $\alpha = 0.65$ for $TCNQ^{\cdot-}$ ARs stacks (the g-factor for $TCNQ^{\cdot-}$ ARs was fixed to $g_{TCNQ} = 2$). The need to account for dimerization suggests that even small changes in TCNQ-TCNQ distances and coplanarity of the quinoide rings in anion-radical stacks may lead to a sufficient

alternation of exchange coupling in the stacks. In addition, the exchange couplings in anion-radical stacks may gradually change due to the temperature-dependent strengthening of AFM exchange coupling at lower temperatures, which cannot be simply taken into account in the used model of the temperature dependence of the susceptibility. Finally, one cannot exclude the influence of π-dimerized $(TCNQ)_2$ units in a disordered structure, which may be coupled by a weaker exchange interaction than are the σ-dimerized dianions $(TCNQ)_2^{2-}$.

4. Conclusions

In this work, the crystal structure of $[Ni(bpy)_3]_2(TCNQ–TCNQ)(TCNQ)_2{\cdot}6H_2O$ (**1**) was studied by single-crystal X-ray structure analyses at 145 K and 100 K in addition to the previous study at 200 K [33]. It was demonstrated that the crystal structures of **1** at these two lower temperatures are essentially the same as the crystal structure studied previously at 200 K. Lowering the temperatures to 145 K and 100 K led to higher proportions of σ-dimerization in the σ- and π-dimerization in the disordered $(TCNQ)_2$ unit and variation of the weaker C–C dimerization σ-bond. In addition, due to lower temperatures, the distance between the two crystallographically independent ARs stacked along the *b*-axis with overlapped exo groups shortened. The quantum chemical calculations corroborated the presence of attractive forces between the two parts of the disordered $(TCNQ)_2$ unit and least energy difference between the σ- and π-dimerization at 200 K in line with lowest proportion of the two forms of dimerization. Temperature-dependent (1.8–270 K) magnetic study of **1** has shown the contribution of Ni(II) ions ($S = 1$) and the contribution of four $S = 1/2$ species carried by TNCQ radicals at higher temperatures, strongly coupled by antiferromagnetic (AFM) exchange interaction at 270 K while at low temperature a negligible contribution of TNCQ radical spins was observed.

Credit author statement

Slavomíra Šterbinská: Investigation, Writing – original draft, Visualization, Validation. **Mariia Holub**: Investigation, Visualization. **Michal Hegedüs**: Investigation, Visualization. **Ján Titiš**: Investigation, Validation, Formal analysis, Review and Editing. **Erik Čižmár**: Investigation, Validation, Formal analysis, Review and Editing, Validation, Supervision. **Larry R. Falvello**: Investigation, Formal analysis, Review and Editing, Validation, Funding acquisition. **Juraj Černák**: Conceptualization, Writing – original draft, Review and Editing, Supervision, Project administration, Funding acquisition.

Declaration of competing interest

The authors declare that they have no known competing financial interests or personal relationships that could have appeared to influence the work reported in this paper.

Acknowledgement

Financial support from Slovak Grant Agencies (APVV-18-0016, VEGA 1/0189/22), internal grants of P. J. Šafárik University in Košice (VVGS-PF-2021-1772 and VVGS-2020-1657) and by the Spanish Ministerio de Ciencia e Innovación (Grant PGC2018–093451-B-I00), the European Union Regional Development Fund, (FEDER), and the Diputación General de Aragón, Project M4, E11_20R.

Appendix A. Supplementary data

Supplementary data to this article can be found online at https://doi.org/10.1016/j.solidstatesciences.2022.106959.

References

[1] D.S. Acker, W.R. Hetler, J. Am. Chem. Soc. 84 (1962) 3370–3374, https://doi.org/10.1021/ja00876a028.
[2] L.R. Melby, R.J. Harder, W.R. Hertler, W. Mahler, R.E. Benson, W.E. Mochel, J. Am. Chem. Soc. 84 (1962) 3374–3387, https://doi.org/10.1021/ja00876a029.
[3] W. Kaim, M. Moscherosch, Coord. Chem. Rev. 129 (1994) 157–193, https://doi.org/10.1016/0010-8545(94)85020-8.
[4] L. Ballester, A. Gutiérrez, M.F. Perpiñán, M.T. Azcondo, Coord. Chem. Rev. 190-192 (1999) 447–470, https://doi.org/10.1016/S0010-8545(99)00098-3.
[5] A. Nafady, A.P. ÓMullane, A.M. Bond, Coord. Chem. Rev. 268 (2014) 101–142, https://doi.org/10.1016/j.ccr.2014.01.017.
[6] V.A. Starodub, T.N. Starodub, Usp. Khim. 83 (2014) 391–438, https://doi.org/10.1070/RC2014v083n05ABEH004299.
[7] S.Z. Goldberg, B. Spivack, G. Stanley, R. Eisenberg, D.M. Braitsch, J.S. Miller, M. Abkowitz, J. Amer. Chem. Soc. 99 (1977) 110–117, https://doi.org/10.1021/ja00443a021.
[8] J.S. Miller, J.H. Zhang, W.M. Reiff, D.A. Dixon, L.D. Preston, A.H. Reis Jr., E. Gebert, M. Extine, J. Troup, J. Phys. Chem. 91 (1987) 4344–4360, https://doi.org/10.1021/j100300a028.
[9] A.H. Reis Jr., L.D. Preston, J.M. Williams, S.W. Peterson, G.A. Candela, L. J. Swartzendruber, J.S. Miller, J. Am. Chem. Soc. 101 (1979) 2756–2758, https://doi.org/10.1021/ja00504a058.
[10] D.M. O'Hare, M.D. Ward, J.S. Miller, Chem. Mat. 2 (1990) 758–763, https://doi.org/10.1021/Cm00012A031.
[11] C. Alonso, L. Ballester, A. Gutiérrez, M.F. Perpinán, A.E. Sánchez, M.T. Azcondo, Eur. J. Inorg. Chem. 3 (2005) 486–495, https://doi.org/10.1002/ejic.200400540.
[12] R. Jain, K. Kabir, J.B. Gilroy, K.A.R. Mitchell, K.-C. Wong, R.G. Hicks, Nature 445 (2007) 291–294, https://doi.org/10.1038/nature05439.
[13] K.I. Pokhodnya, N. Petersen, J.S. Miller, Inorg. Chem. 41 (2002) 1996–1997, https://doi.org/10.1002/(SICI)1521-4095(200003)12:6<410::AID-ADMA410>3.0.CO;2-B.
[14] H. Zhao, R.A. Heintz, X. Ouyang, K.R. Dunbar, C.F. Campana, R.D. Rogers, Chem. Mater. 11 (1999) 736–746, https://doi.org/10.1021/cm980608v.
[15] J. Zhang, P. Yan, G. Li, G. Hou, M. Suda, Y. Einaga, Dalton Trans 47 (2009) 10466–10473, https://doi.org/10.1039/b909213g.
[16] C. Kachi-Terajima, N. Kimura, Y. Tomori, D. Akahoshi, T. Saito, J. Coord. Chem. 71 (2018) 3600–3614, https://doi.org/10.1080/00958972.2018.1521965.
[17] J. Černák, M. Hegedüs, L. Váhovská, J. Kuchár, D. Šoltésová, E. Čižmár, A. Feher, L. R. Falvello, Solid State Sci 77 (2018) 27–36, https://doi.org/10.1016/j.solidstatesciences.2018.01.004.
[18] H. Zhao, M.J. Bazile Jr., J.R. Galán-Mascarós, K.R. Dunbar, Angw. Chem. 115 (2003) 1045–1048, https://doi.org/10.1002/ange.200390234.
[19] G. Wang, C. Slebodnick, G.T. Yee, Acta Cryst C65 (2009) m28–m32, https://doi.org/10.1107/S0108270108041152.
[20] C. Willi, A.H. Reis Jr., E. Gebert, J.S. Miller, Inorg. Chem. 20 (1981) 313–318, https://doi.org/10.1021/ic50216a002.
[21] D.B. Tanner, J.S. Miller, M.J. Rice, J.J. Ritsko, Phys. Rev. B: Cond. Matt. Mat. Phys. 21 (1980) 5835–5845, https://doi.org/10.1103/PhysRevB.21.5835.
[22] D. O'Hare, J.S. Miller, Mol. Cryst. Liq. Cryst. 176 (1989) 381–390, https://doi.org/10.1080/00268948908037496.
[23] J.S. Miller, Angew. Chem. 118 (2006) 2570–2588, https://doi.org/10.1002/ange.200503277.
[24] M. Capdevila-Cortada, J.S. Miller, J.J. Novoa, Chem. Eur. J. 21 (2015) 6420–6432, https://doi.org/10.1002/chem.201406028.
[25] C.R. Groom, I.J. Bruno, M.P. Lightfoot, S.C. Ward, Acta Cryst B72 (2016) 171–179, https://doi.org/10.1107/S2052520616003954.
[26] S. Shimomura, M. Higuchi, R. Matsuda, K. Yoneda, Y. Hijikata, Y. Kubota, Y. Mita, J. Kim, M. Takata, S. Kitagawa, Nat. Chem. 2 (2010) 633–637, https://doi.org/10.1038/nchem.684.
[27] V. Dong, H. Endres, H.J. Keller, W. Moroni, D. Nöthe, Acta Cryst B33 (1977) 2428–2431, https://doi.org/10.1107/S0567740877008668.
[28] B. Adinarayana, D. Shimizu, K. Furukawa, A. Osuka, Chem. Sci. 10 (2019) 6007–6012, https://doi.org/10.1039/C9SC01631G.
[29] T. Kobashi, D. Sakamaki, S. Seko, Angew. Chem. Int. Ed. 55 (2016) 8634–8638, https://doi.org/10.1002/anie.201603409.
[30] D.V. Konarev, S.S. Khasanov, R.N. Lyubovskaya, Russ. Chem. Bull. 56 (2007) 371–392, https://doi.org/10.1007/s11172-007-0063-7.
[31] D.V. Konarev, R.N. Lyubovskaya, Russ. Chem. Bull. 57 (2008) 1944–1954, https://doi.org/10.1007/s11172-008-0261-y.
[32] D.V. Konarev, L.V. Zorina, S.S. Khasanov, E.U. Khakimova, R.N. Lyubovskaya, Russ. Chem. Bull. 60 (2011) 1063–1070, https://doi.org/10.1007/s11172-011-0168-x.
[33] J. Černák, J. Kuchár, M. Hegedüs, Acta Cryst E73 (2017) 8–12, https://doi.org/10.1107/S2056989016019162.
[34] H. Endres, H.J. Keller, W. Moroni, D.Z. Nöthe, Naturforsch 31b (1976) 1322–1325, https://doi.org/10.1515/znb-1976-1005.
[35] O.D. Rigaku, CrysAlis PRO, Rigaku Oxford Diffraction, Yarnton, Oxfordshire, England, 2015.
[36] G.M. Sheldrick, Acta Cryst C71 (2015) 3–8, https://doi.org/10.1107/S2053229614024218.
[37] K. Brandenburg, DIAMOND, Crystal Impact GbR, Bonn, Germany, 2007.
[38] (a) F. Neese, The ORCA program system, Wiley Interdiscip. Rev. Comput. Mol. Sci. 2 (2012) 73–78, https://doi.org/10.1002/wcms.81;
(b) F. Neese, ORCA – An Ab Initio, Density Functional and Semi-empirical Program Package, 2018, Version 4.1.2.

[39] W. Schneider, G. Bistoni, M. Sparta, C. Riplinger, M. Saitow, A. Auer, F. Neese, J. Chem. Theory Comput. 12 (10) (2016) 4778–4792, https://doi.org/10.1021/acs.jctc.6b00523.
[40] G. Knizia, J. Chem. Theory Comput. 9 (2013) 4834–4843, https://doi.org/10.1021/ct400687b.
[41] I. Garcia-Yoldi, J.S. Miller, J.J. Novoa, J. Phys. Chem. 113 (2009) 7124–7132, https://doi.org/10.1021/jp901930s.
[42] S. Stoll, A. Schweiger, J. Magn. Reson. 178 (2006) 42–55, https://doi.org/10.1016/j.jmr.2005.08.013.
[43] W. Duffy, K.P. Barr, Phys. Rev. 165 (1968) 647, https://doi.org/10.1103/PhysRev.165.647.
[44] J.W. Hall, W.E. Marsh, R.R. Weller, W.E. Hatfield, Inorg. Chem. 20 (1981) 1033–1037, https://doi.org/10.1021/ic50218a017.
[45] J.C. Bonner, M.E. Fisher, Phys. Rev. 135 (1964) A640–A658, https://doi.org/10.1103/PhysRev.135.A640.
[46] D.C. Johnston, R.K. Kremer, M. Troyer, X. Wang, A. Klümper, S.L. Bud'ko, A. F. Panchula, P.C. Canfield, Phys. Rev. B 61 (2000) 9558, https://doi.org/10.1103/PhysRevB.61.9558.